Signal Processing 100 (2014) 146–159

Contents lists available at ScienceDirect

Signal Processing

journal homepage: www.elsevier.com/locate/sigpro

Hybrid image fusion scheme using self-fractional Fourier functions and multivariate empirical mode decomposition

J.B. Sharma *, K.K. Sharma [1], Vineet Sahula [1]

Department of Electronics & Communication Engineering, Malaviya National Institute of Technology, Jaipur, Rajasthan, India

ARTICLE INFO

Article history:
Received 6 April 2013
Received in revised form
27 December 2013
Accepted 1 January 2014
Available online 23 January 2014

Keywords:
Image fusion
Multivariate empirical mode decomposition
Fractional Fourier transform
Self-fractional Fourier functions

ABSTRACT

Image fusion has emerged as a promising area of research and a bivariate empirical mode decomposition based fusion scheme has recently been proposed in the literature. In this paper, a hybrid fusion scheme combining self-fractional Fourier function (SFFF) decomposition and multivariate empirical mode decomposition is proposed. In the proposed image fusion technique, images to be fused are decomposed into SFFF images. The SFFF images are further decomposed into intrinsic mode functions (IMFs) using multivariate empirical mode decomposition (MEMD). Corresponding IMFs of same decomposition level of SFFF images are fused using local variance based adaptive weight fusion rule to obtain fused IMF images. The fused image is obtained by applying inverse transformation on fused IMF images. The proposed technique provides flexibility in the number of functions in the SFFF decomposition, transform before SFFF decomposition, and the types of source images (real and complex) to be fused. Simulations are performed for fusion of test images with different SFFF decomposition levels and the results are compared with other existing methods. It is seen that the simulation results are comparable to the existing schemes.

1. Introduction

Image fusion is the process of combining multiple images into a single image to improve the information content of the resulting image [1,2]. The researchers have proposed various image fusion schemes in the spatial as well as transform domains with different fusion rules such as pixel averaging, weighted average, maximum value selection, region energy, region variance and so forth [1–17].

Several fusion approaches using multiscale transform such as the discrete wavelet transforms (DWT) [4,5], the Laplacian pyramid [6], the contrast pyramid [7] and the FFT [8] have been presented in literature. However, multi-resolution transform based techniques do not allow image adaptive representation of local features and results in suboptimal image fusion [11,12].

Fractional Fourier transform (FRFT) is generalization of the FFT and it is used to perform signal analysis into intermediate domains. FRFT based fusion schemes provide additional degree of freedom in optimizing fusion quality due to additional free parameter. Image fusion combining FRFT and nonsubsampled contourlet transform (NSCT) has been presented in [17] to exploit the local feature representation capability of NSCT and intermediate time–frequency representation capability of FRFT.

Recently, an image fusion scheme based on image decomposition using self-fractional Fourier functions (SFFF) is reported in [16]. In this scheme, fusion quality of images is optimized by changing number of decomposition levels and by using some transform before SFFF decomposition. Similarly bivariate EMD (BiEMD) algorithm [28] has also been used for image fusion in [12].

However, BiEMD cannot be used when the two source images to be fused are complex or when more than two

* Corresponding author. Tel.: +91 9414592425.
E-mail addresses: jballabh.sharma@gmail.com (J.B. Sharma), kksharma_mrec@yahoo.com (K.K. Sharma), sahula@ieee.org (V. Sahula).
[1] Tel.: +91 9828777137.

0165-1684/$ - see front matter © 2014 Elsevier B.V. All rights reserved.
http://dx.doi.org/10.1016/j.sigpro.2014.01.001

images are to be fused [14,19]. Multivariate empirical mode decomposition (MEMD) algorithm proposed in [29] is an extension of the BiEMD algorithm [28] which overcomes the limitations of BiEMD.

In this paper a hybrid image fusion scheme based on image decomposition using SFFF and MEMD is presented. The proposed scheme includes, it provides additional degree of freedom in using the transform before SFFF decomposition, number of SFFF decomposition levels and number of images to improve the fusion quality.

The motivation behind combining SFFF with MEMD is that the decomposed components may not be orthogonal to each other in other fusion techniques based on multiscale transforms, but in case of SFFF they are orthogonal to each other and therefore carries independent information. Secondly, signals to be fused may not be bandlimited in conventional Fourier domain, but bandlimited in some FRFT domain. However, SFFF decomposition is not a data adaptive decomposition but, empirical mode decomposition (MEMD) is data adaptive decomposition and decomposing signal into nearly orthogonal (not completely orthogonal) intrinsic mode functions (IMFs). Therefore by combining SFFF decomposition with MEMD, the orthogonal signals are used for fusion algorithm and giving better fusion results from this combination [12–27].

The rest of the paper is organized as follows: In Section 2 background theory related to fractional Fourier transform, self-fractional Fourier functions, empirical mode decomposition and multivariate empirical mode decomposition is presented. In Section 3, the proposed fusion scheme is presented. Section 4 gives the simulation results and the conclusions are given in Section 5.

2. Background theory

2.1. Fractional Fourier transform

The fractional Fourier transform (FRFT) is a generalization of the conventional Fourier transform and the FRFT domains can be interpreted as intermediate domains between spatial and frequency domains [21]. The 2D-FRFT with angles α and β of a signal $f(x, y)$, denoted as $\mathcal{F}^{\alpha,\beta}(u,v)$, is defined as [21]

$$\mathcal{F}^{\alpha,\beta}(u,v)=\int_{-\infty}^{\infty}\int_{-\infty}^{\infty} f(x,y)K_{\alpha,\beta}(x,y,u,v)dx\,dy, \tag{1}$$

where $0<|\alpha|<\pi$ and $0<|\beta|<\pi$ and the inverse 2D-FRFT is given by [21]

$$f(x,y)=\int_{-\infty}^{\infty}\int_{-\infty}^{\infty} \mathcal{F}^{\alpha,\beta}(u,v)K^{*}_{\alpha,\beta}(x,y,u,v)du\,dv, \tag{2}$$

where the 2D-FRFT transform kernel $K_{\alpha,\beta}(x,y,u,v)$ is defined as

$$K_{\alpha,\beta}(x,y,u,v)=\begin{cases}\dfrac{\sqrt{1-j\cot\alpha}\sqrt{1-j\cot\beta}}{2\pi}e^{j\left\{(u^2+x^2)/2\right\}\cot\alpha-jux\csc\alpha}\,e^{j\left\{(v^2+y^2)/2\right\}\cot\beta-jvy\csc\beta} & \text{if } \alpha=\beta\neq N\pi,\ N \text{ is integer}\\ \delta(x-u)\delta(y-v) & \text{if } \alpha=\beta=2N\pi,\ N \text{ is integer}\\ \delta(x+u)\delta(y+v) & \text{if } \alpha=\beta=(2N+1)\pi,\ N \text{ is integer}\end{cases}$$

In (2) the superscript $*$ denotes complex conjugation. The 2D-FRFT reduces to the conventional Fourier transform, when $\alpha,\beta=\pi/2$.The 2D-FRFT can be computed by 1D-FRFT using the separatibility property of it.

2.2. Self-fractional Fourier functions

Self-fractional Fourier function (SFFF) is a function, which is invariant under the fractional Fourier transformation for some angle α [21]. SFFFs are Eigen functions of the corresponding FRFT operator. A function from the Hilbert space of finite energy signals can be represented as a sum of M SFFFs, for an angle $2\pi/M$ [21–25].

The SFFF, signal $F(x)$ of rational order $\alpha=N/M$ is defined as [22–25],

$$F(x)=[F+\cdots+F^{(N/M)}+\cdots+F^{(k-1)N/M}]g(x), \tag{3}$$

where $g(x)$ be any generator function, N and M are integers, and F^{α} is the FRFT operator corresponding to angle α. We can represent $g(x, y)$ through the sum of M orthogonal SFFFs of order M as [18,22,23]

$$g(x,y)=\sum_{L=0}^{M-1}F(x,y)_{L,M}, \tag{4}$$

where

$$F(x,y)_{L,M}=\frac{1}{M}\sum_{k=1}^{M}\exp\left(\frac{j2\pi L(k-1)}{M}\right)\left[R^{(\alpha,\alpha)}g(u,v)\right](x,y). \tag{5}$$

The signal $F(x,y)_{L,M}$ is an SFFF, and $\alpha=2\pi(k-1)/M$, and $R^{(\alpha,\alpha)}$ represents a 2D-FRFT operator with angle α along x and y directions.

2.3. EMD and MEMD

Empirical mode decomposition (EMD) proposed in [26] is a fully data driven technique for multiscale decomposition of a nonlinear and nonstationary signal into finite set of oscillatory components. These oscillatory components are natural frequency components of the signal, called intrinsic mode functions (IMFs) and the coarsest component is termed as residue [26,27]. The IMFs of a given signal are extracted using a process called sifting algorithm [26].

Using the EMD, the input signal $f(x, y)$ is decomposed as [26]

$$f(x,y)=\sum_{j=1}^{n}C_j(x,y)+r(x,y), \tag{6}$$

where $C_j(x,y)$ $j=1,2,....,n$, represent intrinsic mode functions (IMFs), and $r(x, y)$ represent the residue signal.

The details of the EMD algorithm to decompose a signal are available in [26,27]. Because of its capability to separate spatial frequencies and to represent local features intuitively, recently a lot of work has been done for image fusion using EMD [9–15].

For complex signals different approaches for empirical mode decomposition are required. An algorithm which gives more accurate complex (equal real and imaginary part) IMFs is the bivariate EMD (BiEMD) and it is proposed in [28]. The BiEMD algorithm is an extension of the standard EMD algorithm for bivariate signals. The BiEMD facilitate a better comparison between common (relevant) frequency scale images from input data by aligning them within a single complex IMF [12,15].

Multivariate empirical mode decomposition (MEMD) is proposed in [29] for data-adaptive time–frequency analysis of multivariate signals. It is an extension of the BiEMD algorithm for multivariate signals and is used for similar scale decomposition and time–frequency analysis of multichannel signals. In MEMD, the multivariate data may have arbitrary number of channels.

In MEMD multiple n-dimensional envelopes are generated by taking signal projections along different directions in n-dimensional spaces, these envelopes are averaged to obtain the local mean [29]. The process of mapping an input multivariate signal into multiple real valued projected signals, to generate multidimensional envelopes, is yielding n-dimensional rotational modes [29]. These n-dimensional rotational modes correspond to multivariate IMFs. The other details of the MEMD algorithm to decompose a signal are available in [29].

In this paper two dimensional MEMD is computed by converting each source image data into one dimensional data by concatenating their rows and then applying MEMD algorithm [29], yielding 1D-IMFs for each channel. Then 1D-IMFs of each channel are converted back into 2D-IMFs by inverse operation. In case of complex (bivariate) source images, real and imaginary parts are separated as independent real data channels for decomposition. Finally complex IMFs are obtained by combining corresponding real and imaginary part channel IMFs after decomposition. It is mentioned here that in the proposed scheme SFFF decomposed images are complex images.

3. Proposed fusion scheme

In this section we present a novel image fusion technique shown in Fig. 1. This technique is based on decomposition of source images into SFFF images and further decomposition based on MEMD. To be more precise, the source images $g_i(x,y), i=1,2,...,N$ are decomposed into M SFFFs images to obtain $[f_i(x,y)_{M,L}]$, $i=1,2,...,N$ using (4) and (5). These SFFFs images are 2D complex arrays. Each SFFFs image is converted to 1D complex array by concatenating their rows. Then the real and imaginary parts of this 1D array are separated into two real 1D arrays. Similarly all SFFFs images are converted into two 1D arrays. These 1D real arrays are combined to form an n-channel multivariate signal. The MEMD algorithm is applied to this n-variate signal, which yields n-variate common frequency scale IMFs. Common frequency scale

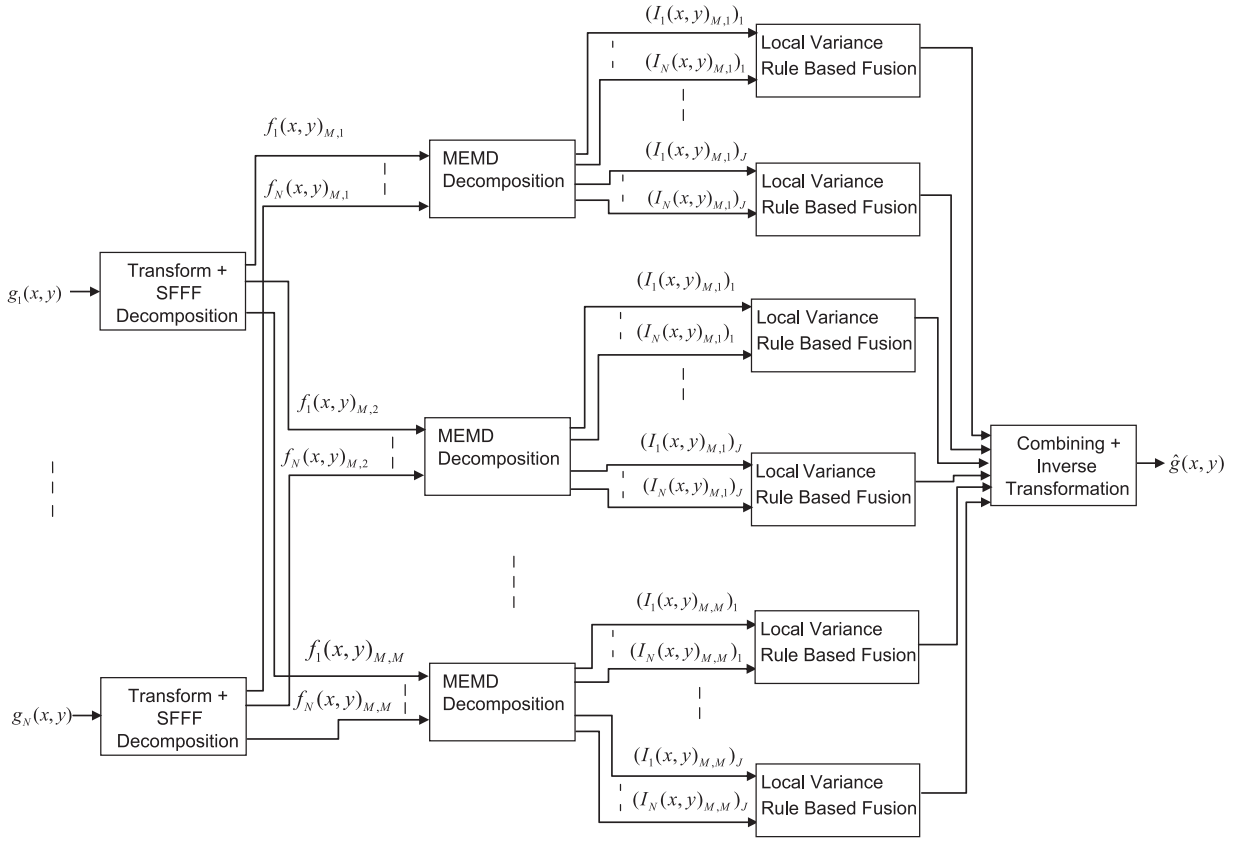

Fig. 1. Block diagram of the proposed fusion scheme.

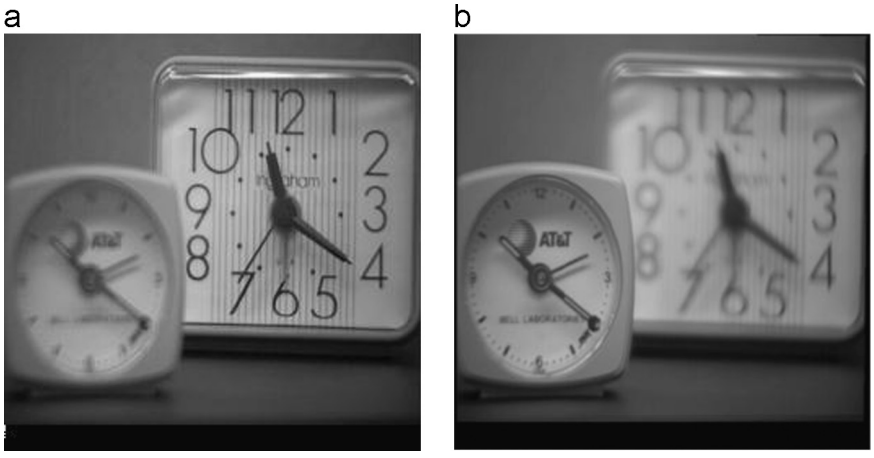

Fig. 2. Out of focus clock image: (a) right focused image and (b) left focused image.

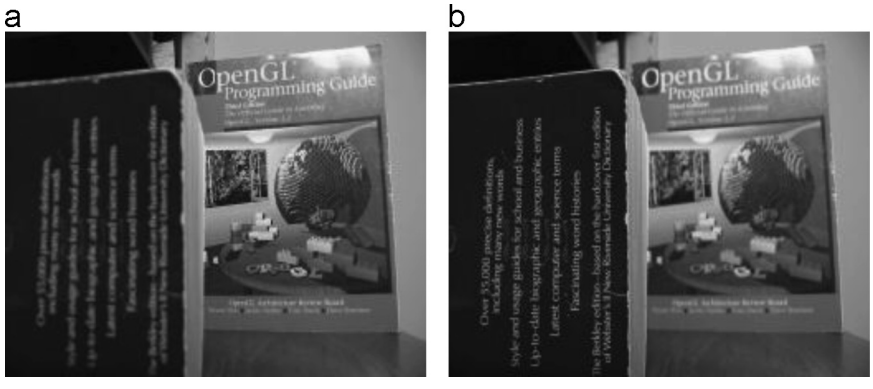

Fig. 3. Out of focus book image: (a) right focused image and (b) left focused image.

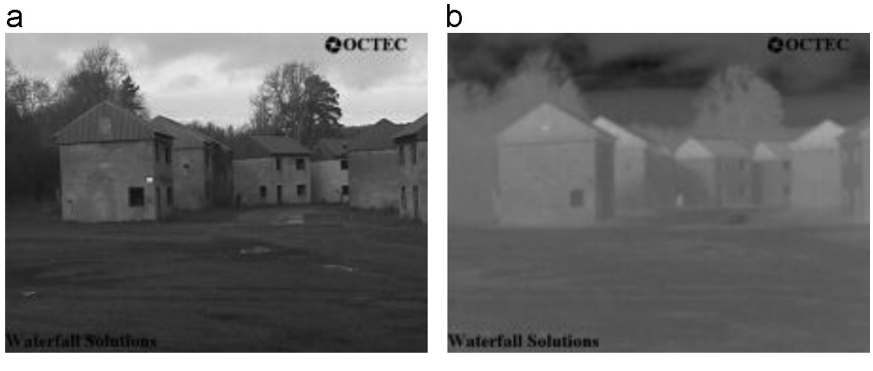

Fig. 4. Multispectral Octec1 image: (a) digital camera image and (b) IR camera image.

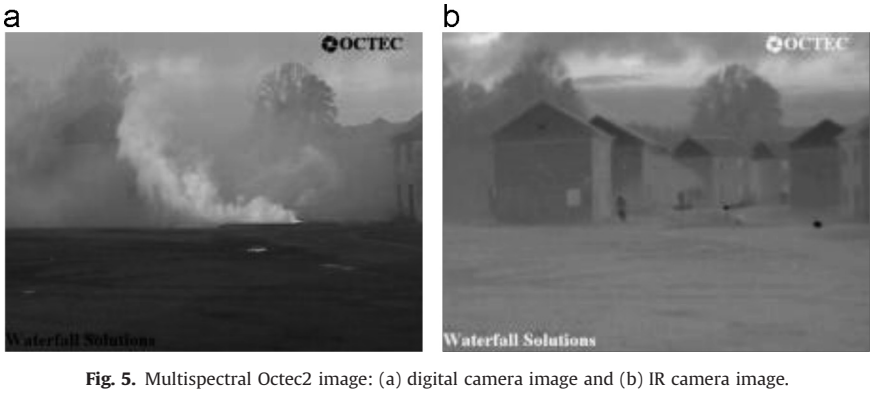

Fig. 5. Multispectral Octec2 image: (a) digital camera image and (b) IR camera image.

IMFs of corresponding real and imaginary part channels are combined to reconstruct complex 1D IMFs and converted back to 2D arrays, denoted as scaled complex IMFs $[(I_i(x,y)_{M,L})_n]$, $n=1,2,...,J$, and $i=1,2,...,N$. This MEMD decomposition is based on (6) and performed for each SFFFs image $[f_i(x,y)_{M,L}]$, $i=1,2,...,N$, where $L=0,1,2,...,M-1$ as shown in Fig. 1. The IMF images obtained from decomposition of SFFFs images of N source images are then combined locally by computing variance of the transformation coefficients at each spatial point for each frequency scale $n=1,2,...,J$ and for the each SFFF decomposition level $L=0,1,2,...,M-1$ of the decomposed images to obtain the fused image $\hat{g}(x,y)$. Local variance based pixel level adaptive weight linear fusion rule is used here for fusion of each IMF image at a particular frequency scale n of a particular SFFF decomposition level L and expressed as

$$[(I(x,y)_{M,L})_n]=\sum_{i=1}^{N}[(\beta_{i(M,L)}(x,y))_n(I_{i(M,L)}(x,y))], \tag{7}$$

where $L=1,2,3,\ldots,M$, and $n=1,2,3,\ldots,J$, the parameters $(\beta_{i(L,M)}(x,y))_n$ are adaptive weights and are determined by local variance based fusion rule reported in [12] and reproduced here as

$$(\beta_{i(M,L)}(x,y))_n=\frac{(\sigma_{i(M,L)}(x,y))_n}{\sum_{i=1}^{N}[(\sigma_{i(M,L)}(x,y))_n]}, \tag{8}$$

where $(\sigma_{i(M,L)}(x,y))_n$ are variances at pixel (x, y) in IMF $(I_{i(M,L)}(x,y))_n$.

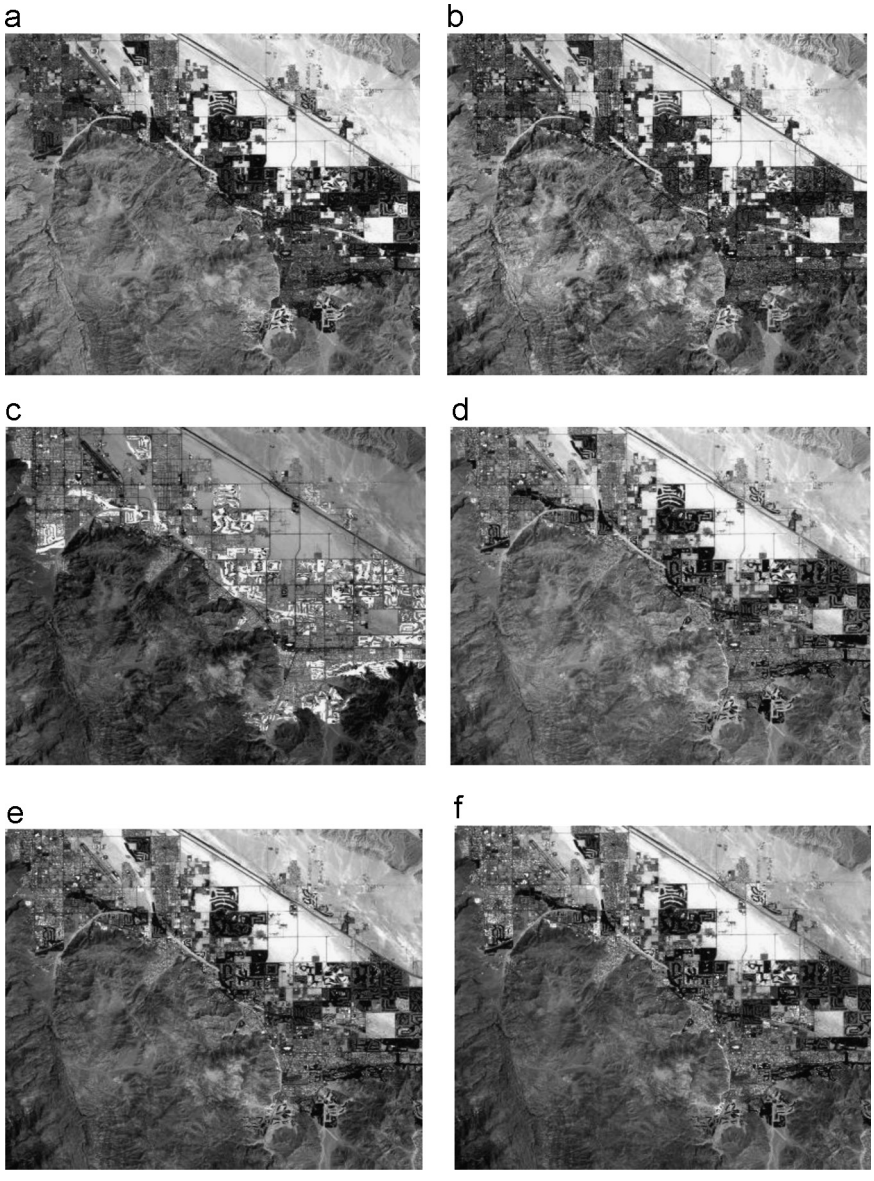

Fig. 6. Multimodal satellite images of band 1, 2, 3, 4, 5 and 7 ((a)–(f)).

The fused IMF images are combined together to obtain fused image $\hat{g}(x,y)$ as given by

$$\hat{g}(x,y) = \sum_{L=0}^{M-1} \sum_{n=1}^{J} (I(x,y)_{M,L})_n. \quad (9)$$

The steps of proposed fusion scheme of Fig. 1 are summarized as follows:

Step 1: Decompose the original source images into M SFFF images.
Step 2: Decompose all SFFF images into complex IMFs using MEMD.
Step 3: The IMFs at a specific order n at a particular SFFF decomposition level L are fused using local variance based adaptive weight linear fusion rule.
Step 4: Fused IMFs are combined and inverse transformation is applied on to obtain final fused image.

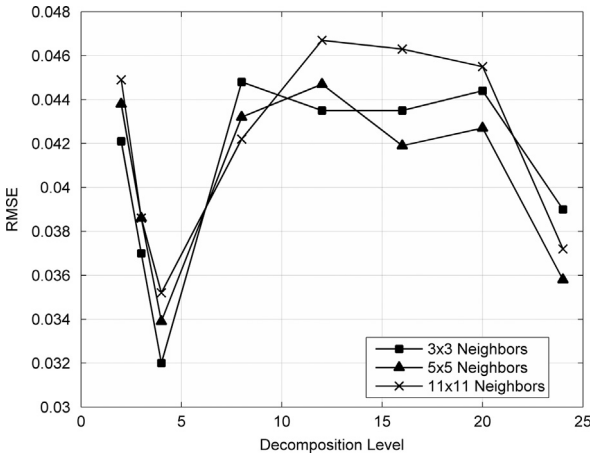

Fig. 8. RMSE vs. SFFF decomposition level with different window sizes for computing local fusion constants for clock image.

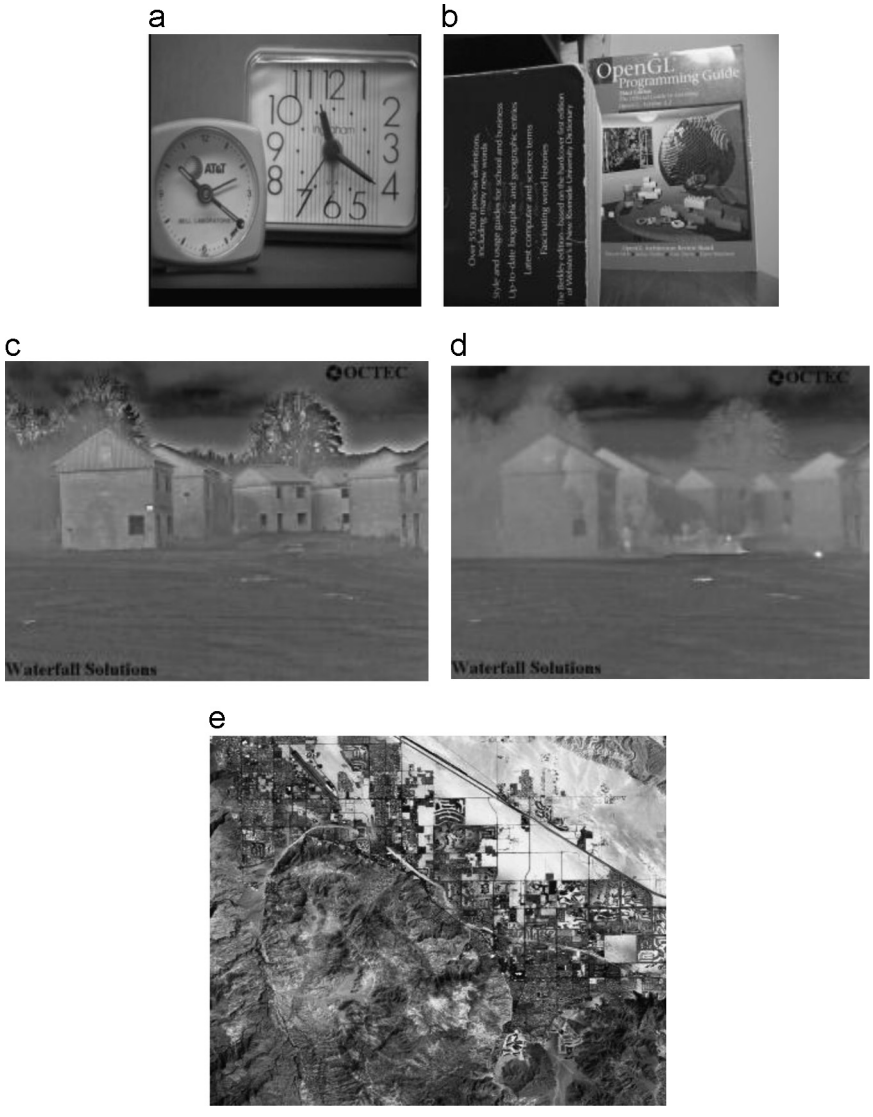

Fig. 7. Reference fused images: (a) clock image, (b) book image, (c) Octec1 image, (d) Octec2 image and (e) landsat TM satellite images.

4. Simulation result

In this section computer simulation results of the proposed fusion scheme performed using MATLAB are presented.

Experiments are performed on three groups of images to validate the efficacy of the proposed scheme. Simulations are also performed to compare the proposed scheme with other fusion schemes such as (i) SFFF alone based scheme [16] using maximum absolute value fusion rule, (ii) MEMD alone based fusion scheme using local variance based adaptive weight fusion rule, which is also equivalent to scheme [12] for two real valued source images [12,29]. Parameters used in simulation of schemes of [16,12] are identical to the parameters reported there. Two performance parameters namely root mean square error (RMSE) and Qabf [35] are calculated and used as objective performance measures for comparison. The quality metric, Qabf, represent the amount of edge information transferred from source images into fused images and the higher values of this metric represent better fusion quality [35].

The RMSE between the reference image (in which both the out of focus images are focused, multispactrum images and multimode images are already fused), and the fused image is calculated. Reference fused images (Fig. 7(a)–(e)) are taken from the fused images available at [20,31–33] respectively. No-reference fusion quality performance matrix, Qabf, is calculated between the source images and the fused image.

First experiment is conducted for fusion of two multi-focus images: "clock" and "book" (Figs. 2(a) and (b), 3(a) and (b)). In this experiment firstly the optimum value of SFFF decomposition level M and the optimum window size W for calculating local variance are estimated.

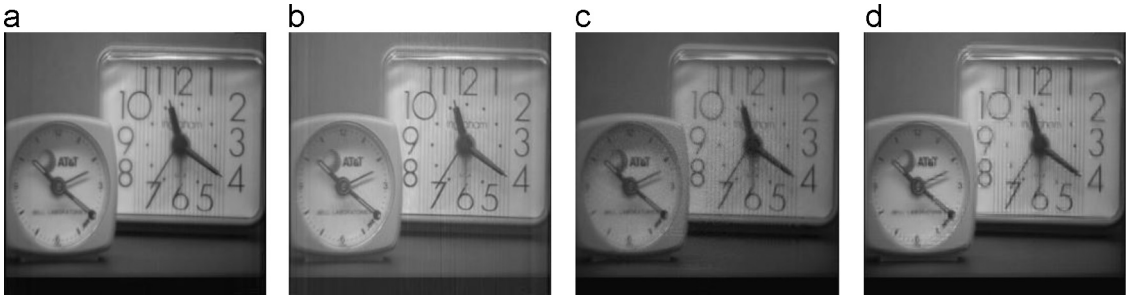

Fig. 9. Fused clock image using: (a) proposed scheme, (b) BiEMD (MEMD alone), (c) SFFF alone and (d) wavelet based scheme.

Fig. 10. Fused book image using: (a) proposed scheme, (b) BiEMD (MEMD alone), (c) SFFF alone and (d) wavelet based scheme.

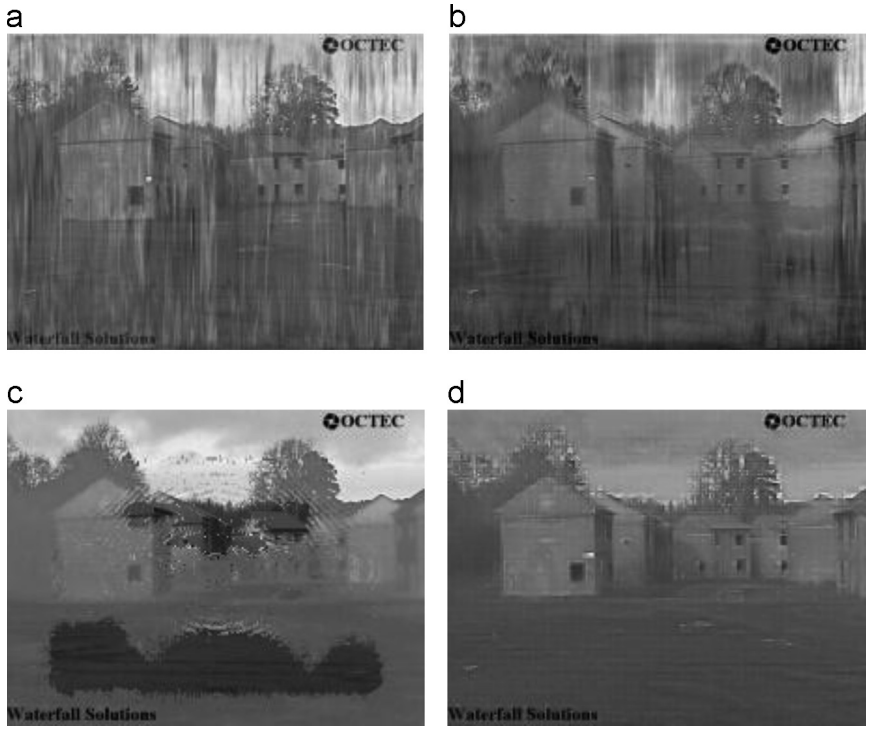

Fig. 11. Fused octec1 image using: (a) proposed scheme, (b) BiEMD (MEMD alone), (c) SFFF alone and (d) wavelet based scheme.

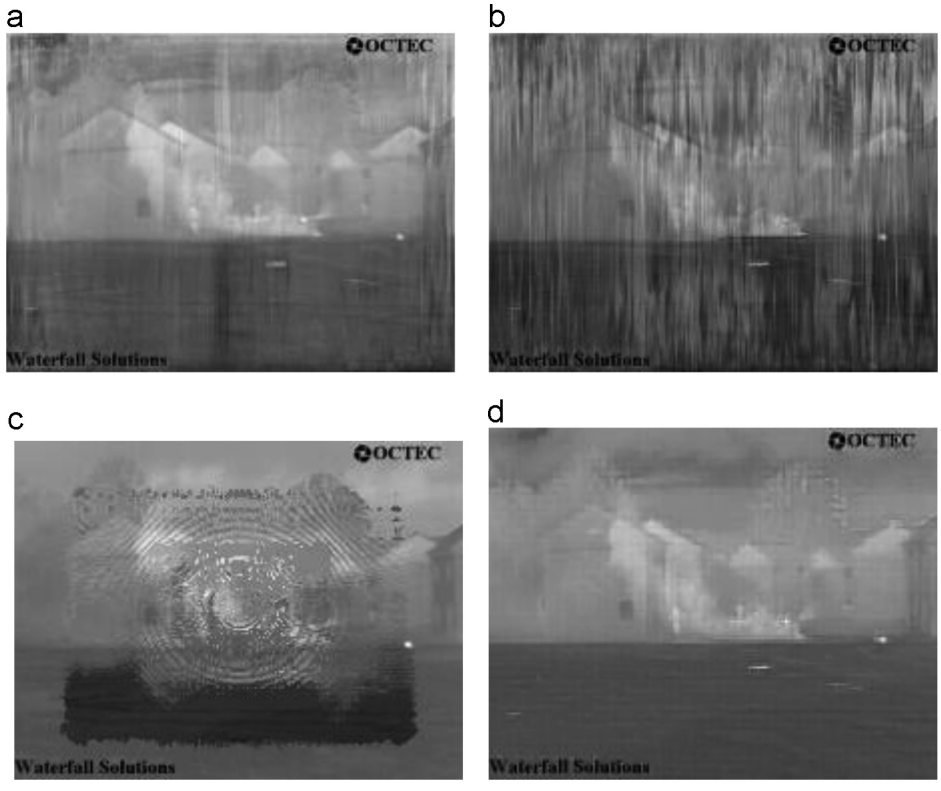

Fig. 12. Fused octec2 image using: (a) proposed scheme, (b) BiEMD (MEMD alone), (c) SFFF alone and (d) wavelet based scheme.

For this the number of SFFF components (M) of clock source images are varied between 2 and 24. The RMSE between fused image and reference image for different values of SFFF decomposition components (M) with different window sizes (W) is computed and is shown in Fig. 8. The RMSE is calculated for $M=2$, 3, 4, 8, 12, 20 and 24 with the fusion local window sizes of $W=3\times3$, 5×5 and 11×11 pixels. It is observed from Fig. 8 that better fusion results for clock image are obtained with $M=4$ and window size $W=3\times3$. For higher value of M, window size of 5×5 gives optimum results. Hence, to conduct fusion experiments, SFFF decomposition level of $M=4$ and window size of $W=3\times3$ are selected as preferred values. For optimization of fusion results, the window size is kept fixed to $W=3\times3$ and the value of M is varied. Simulation results of clock and book images for $M=4$ are shown in Figs. 9(a) and 10(a) respectively. The fusion results of these images for other schemes given in [12,16] are also shown in Figs. 9((b)–(d)), and 10((b)–(d)). It is clear from the results that results of the proposed scheme are comparable to the existing schemes.

In the second experiment, two sets of multispectrum visible and infrared images Octec1 and Octec2 shown in Figs. 4(a), (b) and 5(a), (b) are fused. The improved fusion quality for Octec2 image is obtained for SFFF decomposition level $M=7$ while for image Octec1, $M=4$ gives better results. These simulation results are shown in Figs. 11(a) and 12(a). Fusion results of these images for other schemes compared are also shown in Figs. 11(b)–(c), and 12(b)–(c). It is observed that results of proposed scheme for Octec2 image are better than other existing schemes. For Octec1 image, fusion results are comparable to other schemes.

For third fusion experiment, multimodal Landsat TM images of band 1, 2, 3, 4, 5 and 7 (Fig. 6(a)–(f)) available at [32] are used. The improved fusion results for this image data set is obtained for $M=6$. Simulation results of the proposed scheme, MEMD alone based scheme and scheme [16] are shown in Fig. 13(a)–(c). It is clear that the results of proposed scheme are comparable to the results of MEMD alone based scheme. But the proposed scheme provides freedom to select the decomposition levels and the transform before SFFF decomposition to optimize the fusion quality.

Simulations are also performed using conventional wavelet based fusion scheme [4] using Daubechies's wavelet DBSS (2,2) with two-level decomposition using code given in [31]. The parameters are selected as suggested in [4,34] for the sake of comparison and for evaluating the quality of proposed scheme results. Simulation results for above data set are presented in Figs. 9(d), 10(d), 11(d) and 12(d). It can be observed that the simulation results of the proposed technique are comparable to the results of the wavelet decomposition scheme using Daubechies's wavelet DBSS (2,2).

Computed RMSE for above mentioned experiments are presented in Table 1. It can be observed from this table that the fusion quality is dependent on number of decomposition levels.

Experiments are also performed on some additional images shown in Fig. 14 (Image-1–Image-5) obtained from [33] and the fusion results of these images are shown in Figs. 15–19. In this experiment, the decomposition level is kept fixed at four ($M=4$). Nonreference performance matrix Qabf is computed to measure the fusion quality of these images and results are presented in Table 2. It is observed from Table 2 that the proposed scheme outperforms for three images (Image-2–Image-4) and inferior for two images (Image-1 and Image-5). It is also observed from fused images (Figs. 15(a)–19(d)) obtained using the proposed scheme and the existing schemes that the subjective fusion quality of proposed scheme is comparable to the existing schemes for all images. It may be mentioned here that the objective fusion results can be further improved by changing the decomposition level (M).

The proposed scheme provide additional degree of freedom in using transform before SFFF decomposition, number of SFFF decomposition levels, and number and types of image sensors to improve the fusion quality. The proposed scheme can also be used for complex images like synthetic aperture radar (SAR) and satellite images. But it

Table 1
Comparison of root mean square error (RMSE) of proposed scheme with other schemes.

Fusion Scheme→ Image↓		SFFF+MEMD	MEMD alone	SFFF alone	DWT
CLOCK	$M=4$	0.0320	0.1082	0.0809	0.0379
BOOK	$M=4$	0.0245	0.0417	0.0386	0.0330
OCTEC2	$M=7$	0.1154	0.2408	0.1971	0.1585
OCTEC1	$M=4$	0.1593	0.2081	0.2438	0.1599
Satellite	$M=6$	0.1376	0.1382	0.1456	–

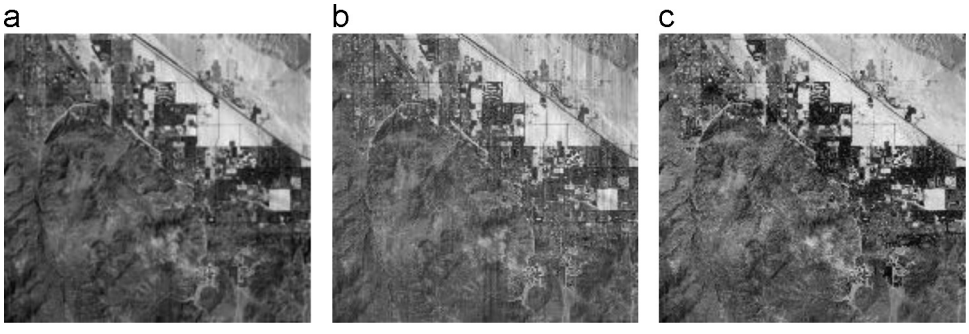

Fig. 13. Fused octec image using: (a) proposed scheme, (b) BiEMD (MEMD alone) and (c) SFFF alone.

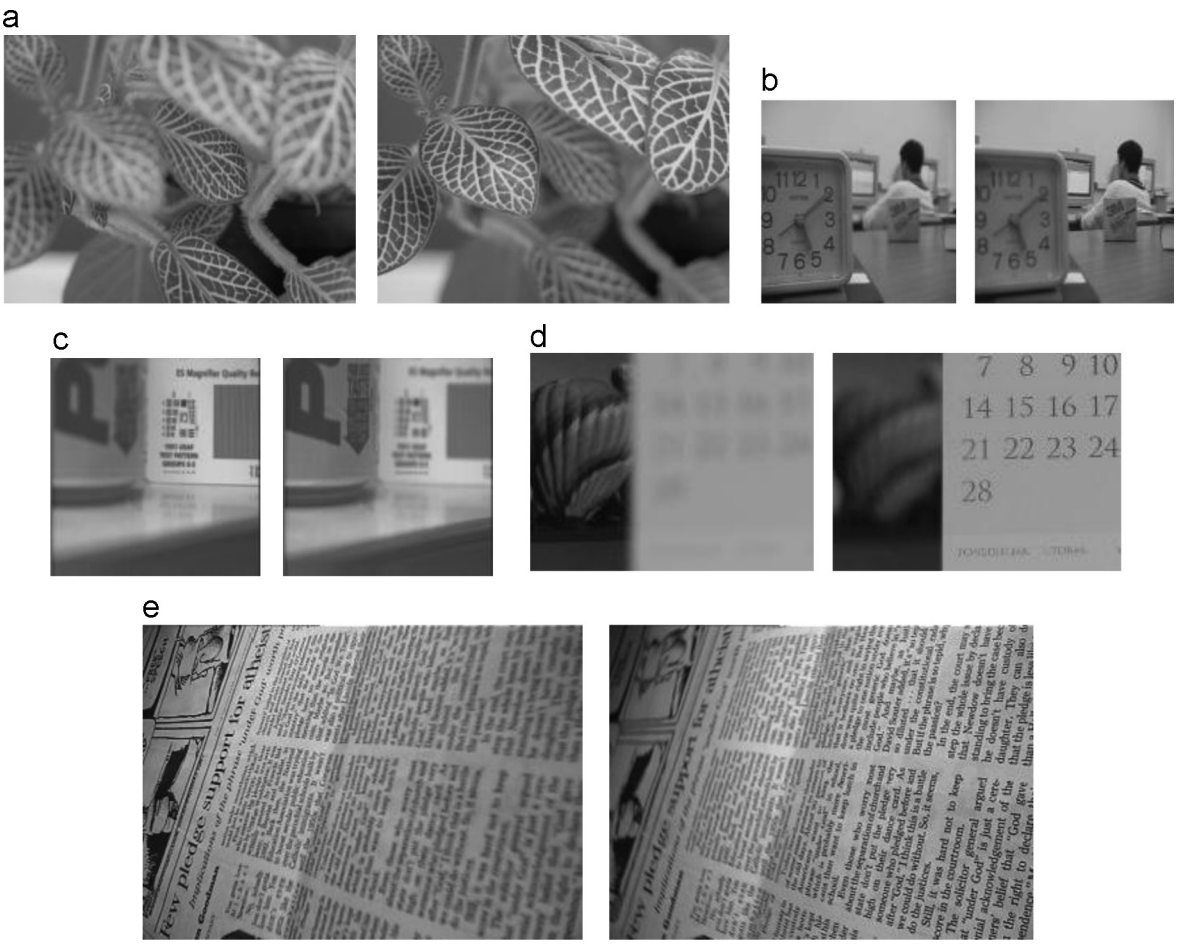

Fig. 14. ((a)–(e)) Five test images used for comparing nonreference performance matrix Qabf of various fusion schemes and referred to as Image-1–Image-5.

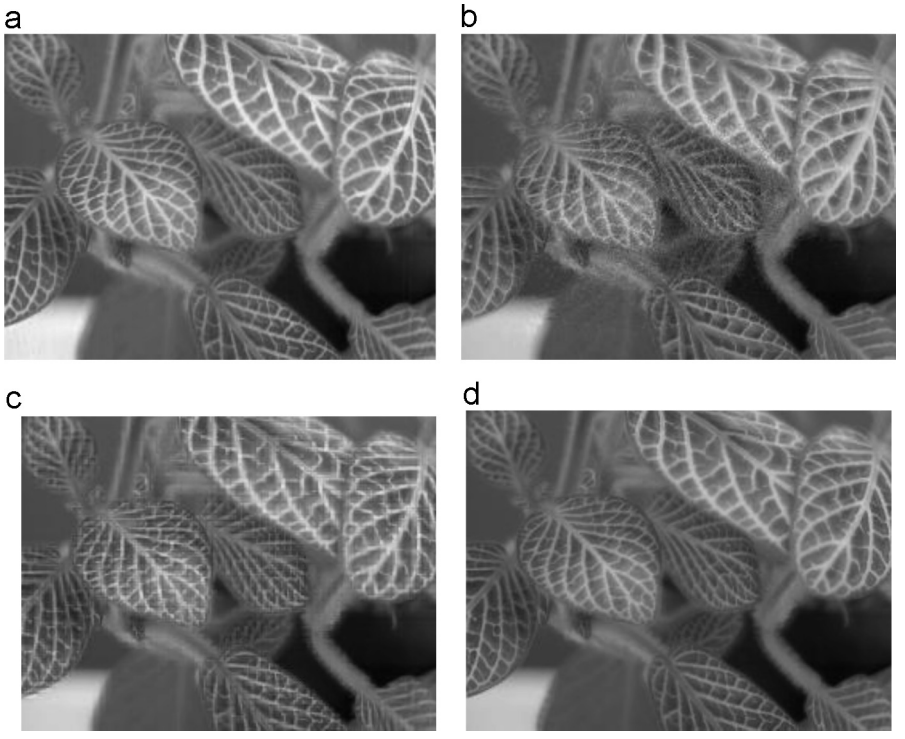

Fig. 15. Fused test image Image-1 using: (a) proposed scheme, (b) BiEMD (MEMD alone), (c) SFFF alone and (d) wavelet based scheme.

has the limitation of higher complexity and computation time.

Computational cost of the proposed scheme is the sum of the cost of SFFF computation and multivariate EMD computation. The computation cost for SFFF decomposition of $N \times N$ size image and M SFFF decomposition levels is $M*N^2 \log_2 N$. For more detail readers can refer [21,22]. Computation cost of MEMD algorithm [28] used in the proposed scheme is mentioned in [30].

Let J, K_n, L and D be the number of extracted IMFs, number of sifting iterations performed to extract nth IMF, data length and multivariate data dimension respectively. Now $d_{n,k}$ represent nth IMF computed at kth iteration of the sifting process, $M_{RM}(d_{n,k}, p)$ the number of extrema detected in the pth projection of $d_{n,k}$ when P projection directions are used.

For given value of L and D the computational complexity $F(d_{n,k+1})$ of one sifting operation necessary to obtain $d_{n,k+1}$ from $d_{n,k}$ is given by

$$F(d_{n,k+1}) = L(2D+18)P + 15 \sum_{p=1}^{P} M_{RM}(d_{n,k}, p). \tag{10}$$

Total computational cost $c(s)$ for a source signal s for MEMD algorithm [28] is obtained by summing the complexity (10) over number of iterations K_n and number of IMFs J and given as

$$c(s) = \sum_{n=1}^{J} \sum_{k=1}^{K_n} F(d_{n,k}). \tag{11}$$

In the proposed fusion algorithm 'i' images of $N \times N$ size and M SFFF decomposition levels are used, therefore $L = N^2, D = 2M*i$. Since the SFFF decomposed images are complex images and each result in two channels here $P = 64$ projection planes are used. Hence, computation cost of one sifting operation $F(d_{n,k+1})$ in simulating MEMD for the proposed algorithm is given as

$$F(d_{n,k+1}) = 64N^2(4M*i + 18) + 15 \sum_{p=1}^{64} M_{RM}(d_{n,k}, p). \tag{12}$$

here $M_{RM}(d_{n,k}, p)$ denotes the number of extrema detected in the pth projection of $d_{n,k}$ which depends upon the image data. Therefore total computation cost is dependent on number of oscillatory components present in the source images.

5. Conclusion

In this paper an image fusion scheme based on SFFF and MEMD decomposition is proposed. In this scheme images are first decomposed into SFFFs. The SFFF sub-images are further decomposed into IMFs by using MEMD

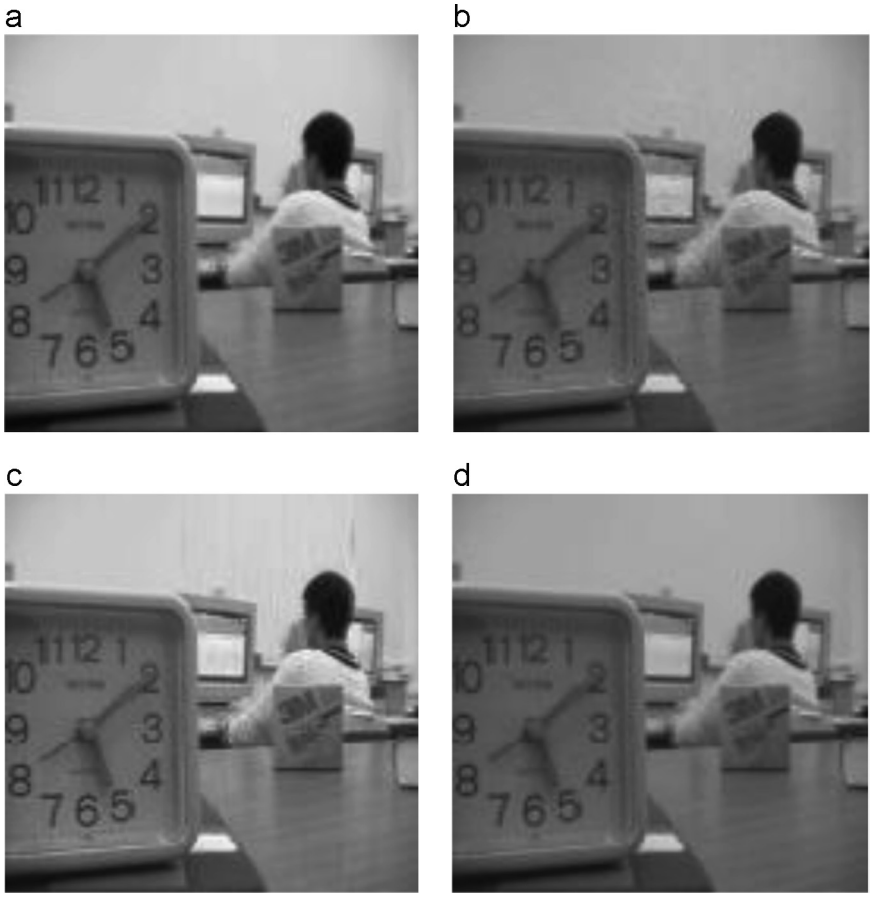

Fig. 16. Fused test image Image- 2 using: (a) proposed scheme, (b) BiEMD (MEMD alone), (c) SFFF alone and (d) wavelet based scheme.

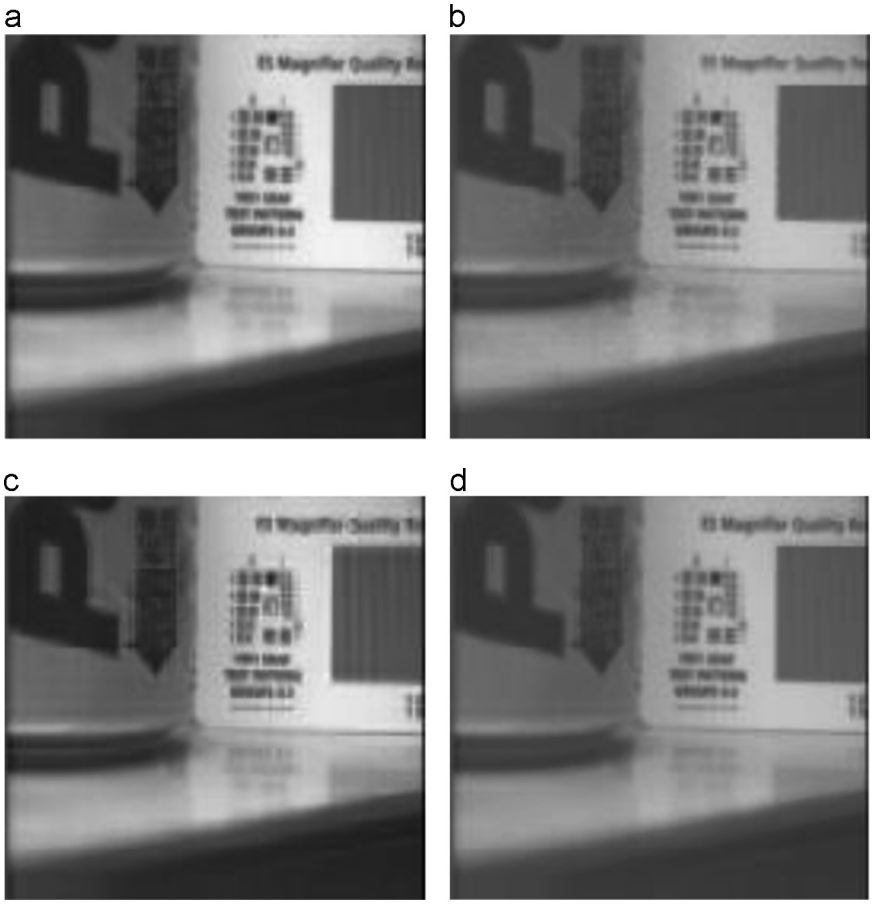

Fig. 17. Fused test image Image 3 using: (a) proposed scheme, (b) BiEMD (MEMD alone), (c) SFFF alone and (d) wavelet based scheme.

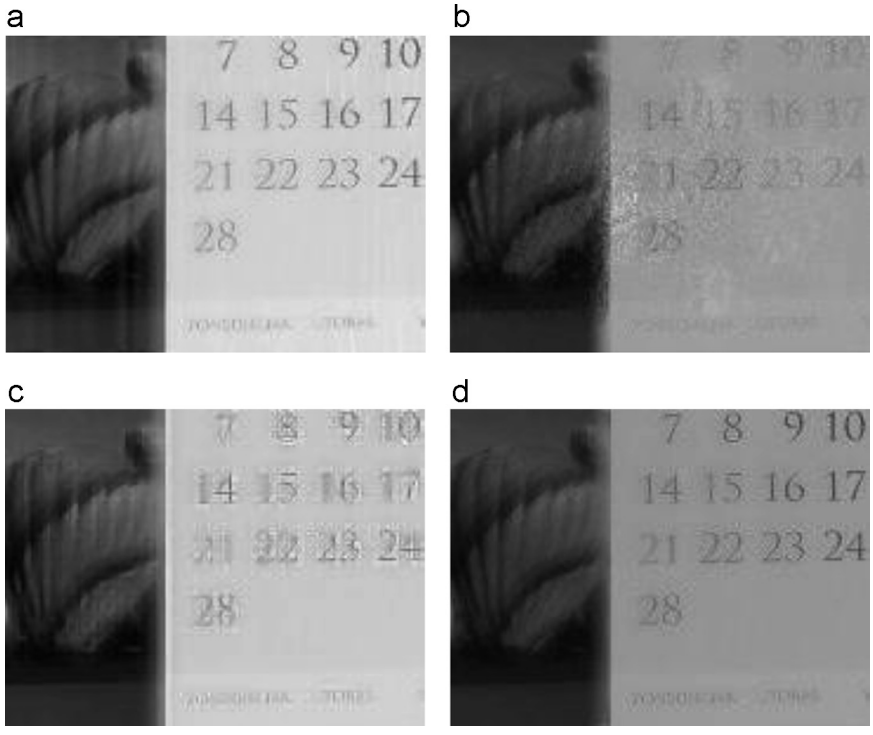

Fig. 18. Fused test image Image-4 using: (a) proposed scheme, (b) BiEMD (MEMD alone), (c) SFFF alone and (d) wavelet based scheme.

Table 2
Comparison of Qabf performance matrix of proposed scheme with other schemes for additional test images (Image-1–Image-5).

Fusion Scheme→ Test Image↓		SFFF+MEMD	MEMD alone	SFFF alone	DWT
Image-1	$M=4$	0.6087	0.6112	0.4129	0.4649
Image-2	$M=4$	0.8240	0.7863	0.7377	0.7530
Image-3	$M=4$	0.7655	0.7180	0.7040	0.7219
Image-4	$M=4$	0.6297	0.6152	0.3722	0.4968
Image-5	$M=4$	0.4301	0.4816	0.3346	0.3114

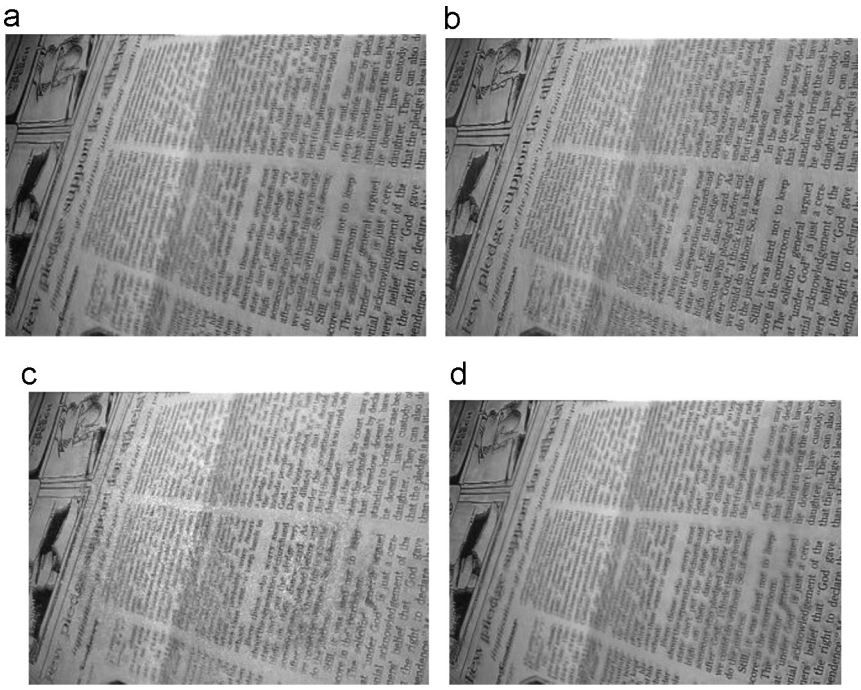

Fig. 19. Fused test image Image-5 using: (a) proposed scheme, (b) BiEMD (MEMD alone), (c) SFFF alone and (d) wavelet based scheme.

and the scale based local fusion rule is applied on corresponding IMFs of same decomposition level SFFF images. The results obtained for four SFFF decomposition levels with 3×3 and 5×5 window sizes are highly encouraging. The proposed scheme also provides flexibility in the use of transform before SFFF decomposition, number of SFFF decomposition levels, multiple fusion rules and number of sensors to improve the fusion quality. The proposed scheme can also be used for n-variate signals such as SAR images, satellite images and n-channel data signals. This scheme however, has the limitation of high computation time and complexity as compared to other existing schemes.

References

[1] Blum, R.S., Liu, Z., Multi-Sensor Image Fusion and Its Applications; special series on Signal Processing and Communications; CRC Press: Boca Raton, FL, USA, 2006.
[2] G. Piella, A general framework for multiresolution image fusion: from pixels to regions, Inf. Fusion 4 (2003) 259–280.
[3] V.P.S. Naidu, J.R. Raol, Pixel level image fusion using wavelets and principle component analysis, Def. Sci. J. 58 (3) (2008) 338–352.
[4] O. Rockinger, Image sequence fusion using a shift-invariant wavelet transform, in: Proceedings of IEEE International Conference on Image Processing, Santa Barbara, CA, October 1997, pp. 288–291.
[5] D.A. Socolinsky, L.B. Wolf, Multispectral image visualization through first order fusion, IEEE Tran. Image Process. 11 (8) (2002) 923–931.
[6] P.J. Burt, E.H. Adelson, The Laplacian pyramid as a compact image code, IEEE Trans. Commun. 31 (4) (1983) 532–540.
[7] A. Toet, L.J. Van Ruyven, J.M. Valeton, Merging thermal and visual images by a contrast pyramid, Opt. Eng. 28 (7) (1989) 789–792.
[8] S. Li, J.T. Kwok, Y. Wang, Combination of images with diverse focus using spatial frequency, Inf. Fusion 2 (3) (2001) 169–176.
[9] H. Hariharan, A. Gribok, M.A. Abidi, A. Koschan, Image fusion and enhancement via empirical mode decomposition, J. Pattern Recognit. Res. I (2006) 16–32.
[10] D. Looney, D.P. Mandic, Fusion of visual and thermal images using complex extension of EMD, in: Proceedings of Second ACM/IEEE International Conference on Distributed Smart Cameras, September 2008, pp. 1–8.
[11] D. Looney, D.P. Mandic, Multiscale image fusion using complex extension of EMD, IEEE Trans. Signal Process. 57 (2009) 1626–1630.
[12] N. Rehman1, D. Looney,T.M. Rutkowski, D.P. Mandic, Bivariate EMD based image fusion, in: Proceedings of IEEE 15th workshop on Statistical Signal Processing, August 2009, pp. 57–60.
[13] D.P. Mandic, George Souretis, David Looney, Marc M. Van Hulle, Toshihisa Tanaka Wai Yie Leong, Complex empirical mode decomposition for multichannel information fusion, IEEE Trans. Signal Process. 57 (4) (2009).
[14] Mosabber Uddin Ahmed, Danilo P. Mandic, Image fusion based on fast and adaptive bidimensional empirical mode decomposition, in: Proceedings of 13th Conference on Information Fusion (FUSION), July 2010.
[15] Foteini Agrafioti, Jiexin Gao, Hoda Mohammadzade, Dimitrios Hatzinakos, A 2D bivariate EMD algorithm for image fusion, in: IEEE Conference on CORFU, 2011, pp. 1–6.

[16] K.K. Sharma, Mohit Sharma, Image fusion based on image decomposition using self-fractional Fourier functions, Signal Image Video Process. (2012). (August).
[17] Hua Peiguang Wang, Tian, Wei Zheng, A Novel Image Fusion Method Based on FRFT-NSCT, Mathematical Problems in Engineering, Hindawi Publishing Corporation, 2013.
[18] K.K. Sharma, Dharmendra Kumar Fageria, Watermarking based on image decomposition using self-fractional Fourier functions, J. Opt. 40 (2) (2011) 45–50.
[19] J.B. Sharma, K.K. Sharma, Vineet Sahula, Digital image dual watermarking using self-fractional Fourier functions, bivariate empirical mode decomposition and error correcting code, J. Opt. 42 (2013) 214–227. (March).
[20] The Image Fusion server, ⟨http://www.imagefusion.org/⟩.
[21] H.M. Ozaktas, Z. Zalevsky, M.A. Kutay, The Fractional Fourier Transform with Applications in Optics and Signal Processing, John Wiley & Sons, Chichester, 2001.
[22] T. Alieva, A.M. Barbe, Self-fractional Fourier functions and selection of modes, J. Phys. A: Math. Gen. 30 (1997) L211.
[23] M.J. Coala, Self-Fourier functions, J. Phys. A: Math. Gen. 24 (1991) L1143.
[24] G. Cincotti, F. Gori, M. Santarsiero, Generalised self Fourier functions, J. Phys. A: Math. Gen. 25 (1992).
[25] T. Alieva, On the self-fractional Fourier functions, J. PhysA: Math. Gen. 29 (1996) L377–L379.
[26] N.E. Huang, Z. Shen, S.R. Long, M.L. Wu, H.H. Shih, Q. Zheng, N.C. Yen, C.C. Tung, H.H. Liu, The empirical mode decomposition and the Hilbert spectrum for nonlinear and nonstationary time series analysis, Proc. R. Soc. A 454 (1998) 903–995.
[27] Z. Wu, N.E. Huang, A study of the characteristics of white noise using the empirical mode decomposition method, Proc. R. Soc. A 460 (2046) (2004) 1597–1611.
[28] G. Rilling, P. Flandrin, P. Goncalves, J.M. Lilly, Bivariate empirical mode decomposition, IEEE Signal Process. Lett. 14 (2007) 936–939. (December).
[29] N. Rahman, D.P. Mandic, Multivariate empirical mode decomposition, Proc. R. Soc. A 466 (May) (2010) 1291–1302.
[30] Julien Fleureau, Amar Kachenoura, Laurent Albera, Jean-Claude Nunes, Lotfi Senhadji, Multivariate empirical mode decomposition and application to multichannel filtering, Signal Process. 91 (2011) 2783–2792. (December).
[31] ⟨http://www.metapix.de/toolbox.htm⟩.
[32] ⟨http://www.imgfsr.com/ifsr_if.html⟩.
[33] ⟨http://www.dsp.etfbl.net/mif/⟩.
[34] Jing Tian, Li Chen, Adaptive multifocus image fusion using a wavelet-based statistical sharpness measure, Signal Process. 92 (2012) 2137–2146.
[35] C.S. Xydeas, V. Petrovic, Objective image fusion performance measure, Electron. Lett. 36 (2000) 308–309. (February).